Seismic scale basement structural mapping in Santos Basin.

Plawiak, R.A.B.[1]; Ferraz, A.E.P.P.D.[1]; Ferrari, A.L.[1]; Mepen, M.[2]; Gambôa, L.A.P.[1]
1- Universidade Federal Fluminense - UFF; 2- Petrogal Brasil S.A.

Abstract

The seismic scale basement structural map of Júpiter area in Santos Basin is presented. It is compared with regional scale gravimetric data to verify the density response that might corroborate the structural basement highs observed in seismic interpretations. A descriptive structural analysis of Júpiter syn-rift faults, interpreted on 3D seismic survey, is reported. Possible reactivations of structures are discussed and may be helpful tools for the understanding of fluid migration at depth.

Introduction

The Santos Basin is widely known for its massive hydrocarbon production in Lower Cretaceous carbonates since 2006, with Tupi discovery. However, in 2008 some exploratory wells reached up to 80% CO_2 concentrations. This is the case of the Júpiter prospect, adjacent to the Tupi field (Figure 1). The latter showed low CO_2 contents with similar geological and structural features from Júpiter (Gamboa et al., 2019). Besides Júpiter, other areas of the basin have stated high CO_2 occurences (Freitas et al., 2022), and their production have been postponed due to several risks (e.g. corrosion of flow lines). The mantelic and magmatic origin of the Santos Basin CO_2 anomalies was interpreted integrating geological and geophysical data with C^{13}/C^{12} isotope geochemical analysis (Santos Neto et al., 2012). Analysing magnetic and gravimetric regional data, Gamboa et al., (2019) proposed that deep faults could possibly be the way for migration of this gas to the pre-salt hidrocarbon reservoirs, in areas of highly stretched continental crust and magmatic intrusions connected to the mantle CO_2 degassing.

The basement of Santos Basin is composed of Neoproterozoic-Cambrian metamorphic rocks from the NE-SW Ribeira Orogenic Belt (Heilbron et al., 2008). As the Gondwana Supercontinent started to break up in Early Cretaceous, intense basaltic volcanism occurred due to early stretching of the crust, developing the rift phase between South America and Africa in Hauterivian (Moreira et al., 2007). The top mapeable signature of these basalts is the focus of this study, known as economic or seismic basement. To corroborate its seismic signature, gravity data are useful to indicate structural highs and lows, as the density contrast between the basalts and the sediments above them allow the generation of gravity anomalies (Gamboa et al., 2021).

As the South Atlantic margin inherited NE-SW orientation from Late Proterozoic structures, the syn-rift architecture resulted in a oblique orientation to the margin (Meisling et al., 2001). This NE-SW inheritance associated with WSW-ENE rift extension, have created segmented faults with sinuous rombo-shaped and left-lateral *en échelon* patterns, as observed and modeled in the East African Rift System (Zwaan and Schreurs, 2017) and in the Central Santos Basin (Pereira et al., 2021).

In the post-rift phase, at least three events of reactivation of syn-rift structures have been observed in a broad range of data: Late Cretaceous, Eocene and Miocene, as a response to Andean orogeny and compression (Cobbold et al., 2001; Fetter, 2009) or as a response to purely gravitacional tectonism (Zalán & Oliveira, 2005). These reactivations have important consequences for burial, maturation and preservation of hydrocarbons (Cobbold et al., 2010) and also for hydrotermal vent formations (MaGee et al., 2016). Although there is no clear concentration of fault reactivation in a specific horizon, or unit, resulting in non-selective reactivations (Alves et al., 2017).

This study aims to present the top seismic scale basement structural map of Júpiter and its clear correlation to gravimetric Bouguer regional scale anomalies. Structural styles of syn-rift faults, possible post-rift reactivation features and depth-slice lineaments are described and discussed.

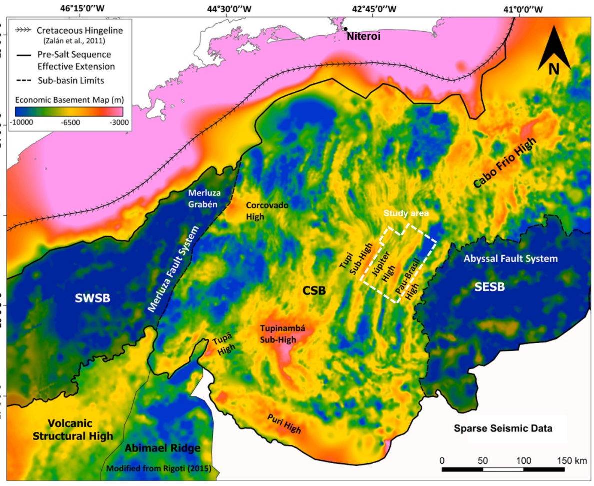

Figure 1 – Study area in Santos Basin. Regional Top Basement Structural Map: basement highs in hot colors and depocenters in cold colors. Sub-basins: SWSB (Southwest Santos), CSB (Central Santos), SESB (Southeast Santos). (adapted from Freitas et al., 2022).

Data and Methods

A Post Stack Depth Migrated (PSDM) 3D seismic reflection survey, in Júpiter area, was used for the interpretations on top basement horizon and syn-rift faults. Decision Space® Geosciences (DSG) software by Landmark was used to perform it. The top basement grid map was generated with Dynamic Framework to Fill™ Workspace from DSG software, using the algorithm Refinement Gridding, a method that uses a minimum curvature algorithm applied to regular grids. The gridding was slightly smoothed at the Júpiter High (JH) for better comparison with gravity anomalies, unaffecting the structural patterns. The Azimuth seismic atribute was generated in DSG, in order to highlight broad structural patterns, using Semblance color chart (blue/black) for better visualization of structures in depth slice views.

The Bouguer gravity data was obtained from the Topex/Poseidon mission, available online in htpps://topex.ucsd.edu, and the first vertical derivative was calculated with Geosoft software (Oasis Montaj® by Seequent), in order to eliminate regional wavelengths, and then highlights the basement related anomalies.

Results

The seismic scale top basement relief map is presented in figure 2. The structural highs form several elongated and sinuous structures, as the depocenters between them. JH is the most proeminente structural high, reaching up to 6 Km in width and almost 50 Km in length.

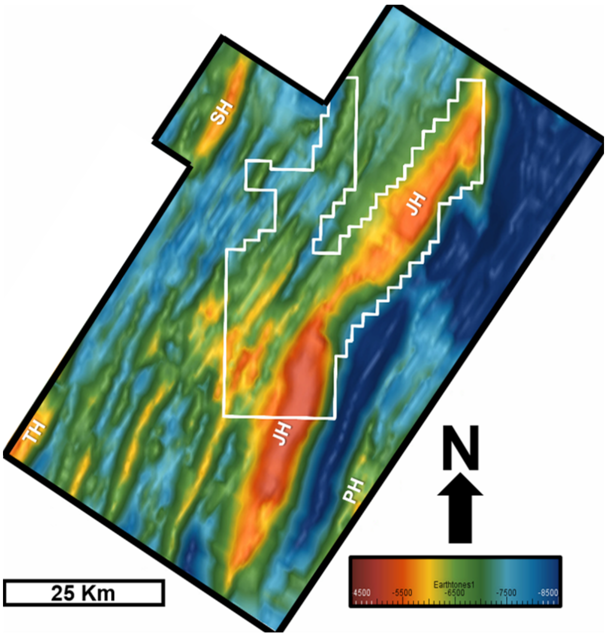

Figure 2 –. Seismic scale top basement relief map. Structural highs in hot colors and depocenters in cold colors. Júpiter prospect in white. JH: Júpiter High; TH: Tupi High; PH: Pau Brasil High; SH: Sépia High.

The Bouguer anomaly vertical derivative revealed excelent correlation with Júpiter High and other main highs (Figure 3). Although, it appears to be smoothed because of regional scale from potential field data.

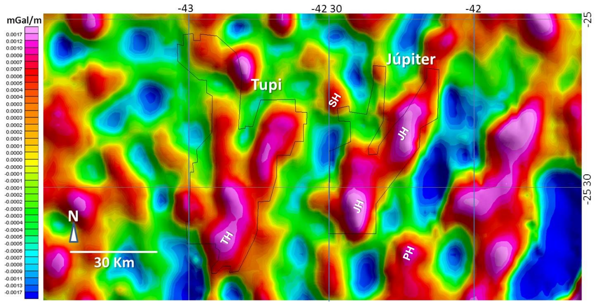

Figure 3 - First vertical derivative from Bouguer gravity anomaly in Tupi field and Júpiter prospect. The hot colors indicate gravimetric highs, with excelent correlation to basement highs, as the depocenters fit to the gravimetric lows in cold colors.

Figure 4 presents the seismic scale top basement structural map of Júpiter. The syn-rift faults are clearly segmented, showing rectilinear to sinuous patterns, varying in strike direction from N to NNE. Although sets of faults exhibited distinct styles, allowing the separation of two structural domains: Northwest (NW) and Southeast (SE) (Figure 4).

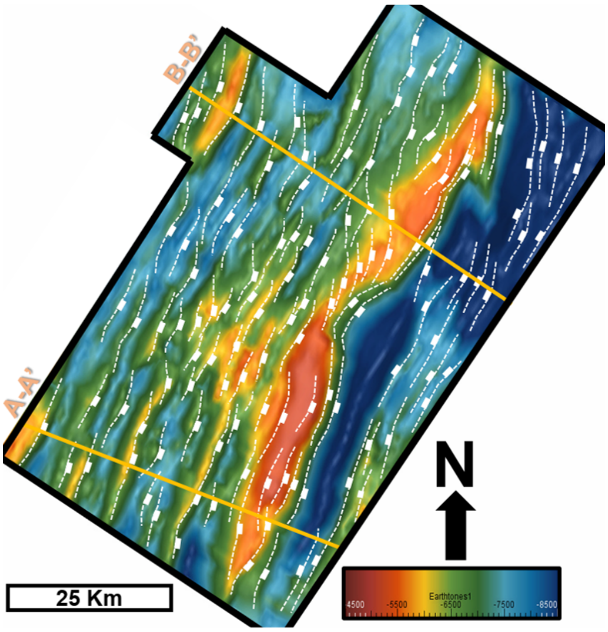

Figure 4 – Top Basement Structural Map. Syn-rift faults (white dashed lines) with dip azimuth indications. Dip sections locations in orange lines.

NW Domain – *en échelon* and rombo-shaped (sigmoidal) styles in map view, with relay ramps stepping the faults segments. In section view, structural styles comprehend extensional planar rotational fault blocks (domino style), forming hemi-grabens with mean dips 30° (Figure 5). Depocenters thicknesses reach up to 2 Km. Top basement deeper depths are thereabout 8 Km.

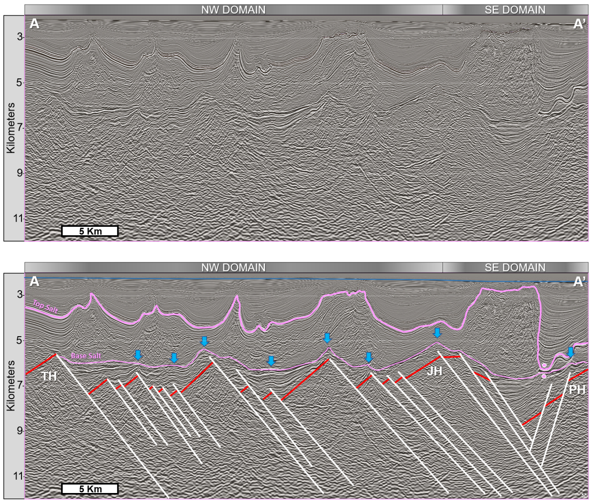

Figure 5 – WNW-ESE Dip direction seismic section. Vertical exaggeration = 2. A salt weld is observed in SE Domain. Top basement in red. Blue arrows pointing out conical-shape structures related to fault tips propagations.

SE Domain – In map view, the fault styles show rectilinear to curved patterns, less segmented than NW Domain, and low angle synthetic and antithetic faults. In section view, structural styles comprehend negative flower-like structures with synthetic faults mean dips 35° and antithetic mean dips 55° (Figure 6). Depocenter thicknesses reach up to 5 Km, salt welds occur in the southernmost corner of the study area, and top basement deeper depths are thereabout 11 Km.

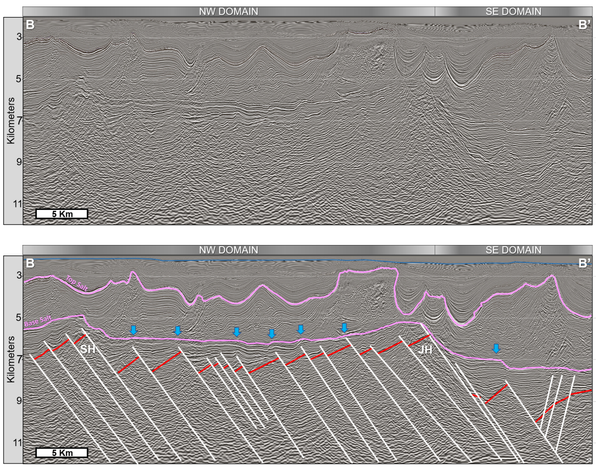

Figure 6 – NW-SE Dip direction seismic section. Vertical exaggeration = 2.2. Top basement in red. Blue arrows pointing out fault-related structures.

The blue arrows in figures 5 and 6 highlight some fault-related structures, clearly connected to the faults tips propagations. Some of these structures occur at the base salt, as the conical-shaped, resembling build ups in section view and fissure ridges in map view. Others occur between top basement and base salt horizons, showing volcanic-like cones and chimneys, also folding and cutting some layers above fault tips.

Two sets of lineaments were identified in depth slices: NNW-SSE and NE-SW, both oblique to the main N-NNE strike direction of syn-rift faults (Figure 7). They occur in a broad range of depth slices, and clearly are crossing over the syn-rift faults with *en échelon* patterns in map view. Interesting to note that NE-SW lineaments highlighted in figure 7 denotes an inflexion axis of the syn-rift strike trends from South to North: NNE and NE-SW trends.

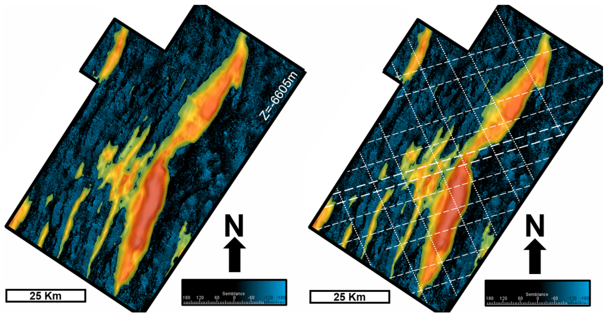

Figure 7 – NNW-SSE and NE-SW *sets of lineaments identified with Azimuth atribute at Z=-6605m.*

Discussion and Conclusions

Excelent correlation between seismic and gravimetric data was observed, showing that integration is fundamental and must be used to corroborate interpretations at diferent scales. Also indicates that gravity interpretation could be used with confidence to previously identify the contrast between sediments and basaltic basement in areas without seismic data.

The structural styles observed in the Hauterivian seismic basement corroborate the strain response to WSW-ENE extension of the South Atlantic oblique rift, closely related to the NE-SW trend inherited from Neoproterozoic-Cambrian Basement structures. This relationship caused left-lateral *en échelon* patterns with segmentation of normal faults distributed as rombo-shaped accommodation zones (relay ramps).

The fault-related features highlighted in figures 5 and 6 are widespread in the study area, and its spatial and temporal distribution may indicate fault reactivations responsible for fluid migration at depth, speccially mantle-derived CO_2. The deeper depocenters observed in SW Domain may indicate a long-term deformation caused by deep crust faulting in a higlhy streched continental crust.

The lineaments identified in depth slices are clearly affecting the syn-rift structural trends. The NE-SW trend may be related to left-lateral movements, but further data integration must be achieved for more detailed investigation, checking seismic signatures with regional magnetic and gravimetric anomalies.

Acknowledgements

This work is part of RD&I Project "Compreendendo as Acumulações de CO_2 na Bacia de Santos/Platô de São Paulo no Contexto da abertura do Atlântico Sul.", financed by Petrogal Brasil S.A., under regulation of Agência Nacional do Petróleo (ANP). The authors are grateful to: Petrogal Brasil S.A., for financing suport and publishing permission; ANP and UFF research group.

References

Alves T, Fetter M, Lima C., Cartwright J., Cosgrove J., Gangá A., Queiroz C., Strugale M. 2017. An incomplete correlation between pre-salt topography, top reservoir erosion, and salt deformation in deep-water Santos Basin (SE Brazil). *Marine and Petroleum Geology* (79), 300-320.

Cobbold P.R., Meisling K.E., Mount S.V., 2001. Reactivation of an obliquely-rifted margin: Campos and Santos basins, SE Brazil. *AAPG Bulletin,* 85:1925-1944.

Cobbold P.R, Chiossi D., Green P.F., Japsen P., Bonow J. 2010. Compressional Reactivation, Atlantic Margin of Brazil: Structural Styles and Consequences for Hydrocarbon Exploration. *Search and Discovery*, Article #30114.

Fetter M. 2009. The role of basement tectonic reactivation on the structural evolution of Campos Basin, offshore Brazil: Evidence from 3D seismic analysis and section restoration. *Marine and Petroleum Geology*, 26:873-886.

Freitas V.A., Vitala J.C.S., Rodrigues B.R., Rodrigues R., 2022. Source rock potential, main depocenters, and CO_2 occurrence in the pre-salt section of Santos Basin. *Journal of South American Earth Sciences*, 115-103760.

Gamboa L., Ferraz A., Baptista R., Santos Neto E.V. 2019. Geotectonic Controls on CO_2 Formation and Distribution Processes in the Brazilian Pre-Salt Basins. *Geosciences*, 9:252.

Gamboa L.A.P., Ferraz A.E.P.P.D., Drehmer L.H., Demercian L.S. 2021. Seismic, magnetic, and gravity evidence of marine incursions in the Santos Basin during the early Aptian, *In* Mello M.R., Yilmaz P.O., Katz B.J. (eds.) The supergiant Lower Cretaceous pre-salt petroleum systems of the Santos Basin, Brazil. *AAPG Memoir*, 124:257-272.

Heilbron M., Valeriano C., Tassinari C.G., Almeida J.C.H., Tupinamba M., Siga Jr. O., Trouw R.A.J. 2008. Correlation of Neoproterozoic terranes between the Ribeira Belt, SE Brazil and its African counterpart: comparative tectonic evolution and open questions. *In*: Pankhurst, R.J., Trouw, R.A.J., Brito-Neves, B.B., de Wit, M.J. (Eds.), West Gondwana: Pre-cenozoic Correlations across the South Atlantic Region, Geological Society, London, Special Publications, 294, pp. 211e237.

Magee C., Duffy O.B., Purnell K, Bell R.E, Jackson C.A.L., Reeve M.T. 2016. Fault-controlled fluid flow inferred from hydrothermal vents imaged in 3D seismic reflection data, offshore NW Australia. *Basin Research,* 28:299-318.

Meisling K.E., Cobbold P.R., Mount V.S. 2001. Segmentation of an obliquely-rifted margin, Campos and Santos basins, Southeastern Brazil. *AAPG Bulletin*, 85 (11):1903-1924.

Moreira J.L.P., Madeira C.V., Gil J.A., Machado M.A.P. 2007. Bacia de Santos. *Boletim Geociências Petrobras.* 15(2):531-549.

Pereira C.E.L., Gomes C.J.S, Araújo M.N.C. 2021. A influência de estruturas preexistentes na formação de riftes oblíquos: o uso da modelagem física e sua comparação com a fase Pré-sal da Bacia de Santos, Brasil. *Geol. USP, Sér. cient*., São Paulo, v. 21, n. 4, p. 110-124.

Santos Neto E.V., Cerqueira J.R., Prinzhofer A. 2012. Origin of CO_2 in Brazilian Basins. *AAPG Annual Convention and Exhibition*. Long Beach, CA.

Zwaan F. and Schreurs G. 2017. How oblique extension and structural inheritance influence rift segment interaction: Insights from 4D analog models. *Interpretation*, 5:1, p. SD119–SD138